HOKKAIDO UNIVERSITY

| | |
|---|---|
| Title | Teraheltz Response of Schottky Wrap Gate-Controlled Quantum Dots |
| Author(s) | Kasai, Seiya; Han, Weihua; Yumoto, Miki et al. |
| Citation | Physica Status Solidi. C. Current Topics in Solid State Physics, 0(4), 1329-1332<br>https://doi.org/10.1002/pssc.200303083 |
| Issue Date | 2003-06-26 |
| Doc URL | https://hdl.handle.net/2115/8457 |
| Rights | Published in "Physica Status Solidi. C. Current Topics in Solid State Physics", volume 0, issue 4, 1329-1332 (26 Jun 2003). |
| Type | journal article |
| File Information | QD02_G29.pdf |

Hokkaido University Collection of Scholarly and Academic Papers : HUSCAP

# Teraheltz Response of Schottky Wrap Gate-Controlled Quantum Dots

**Seiya Kasai***, **Weihua Han, Miki Yumoto and Hideki Hasegawa**

Research Center for Integrated Quantum Electronics and Graduate School of Electronics and Information Engineering, Hokkaido University, N13, W8, Kita-ku, Sapporo, 060-8628 Japan

Received 1 October 2002, revised 6 November 2002, accepted 2002
Published online

**PACS** 73.63.Kv

THz responses of Schottky wrap gate (WPG)-controlled quantum dots were investigated. Normal incidence THz irradiation on single-dot and multi-dot devices with a $CH_3OH$ laser (2.54 THz) changed conductance behavior and produced an additional conductance peak in the *I-V* characteristics of WPG single electron transistors (SETs) at 5 - 20K. The effect depended on the THz electric field polarization. The observed behavior was explained by photon assisted tunneling based on Tien-Gordon theory.

## 1 Introduction

Solid-state devices operating in the so-called "THz gap" region of electromagnetic waves are highly demanded for possible applications in advanced information technology (IT), biochemistry, nanotechnology and so on. Semiconductor quantum dots have high potentials for solid-state THz devices, since their energy scales such as subband spacing fall in a few meV range, corresponding to THz frequencies.

This paper investigates THz response of Schottky wrap gate (WPG)-controlled semiconductor quantum dots in view of application to solid-state THz devices.

The WPG structure and WPG-controlled quantum dot are schematically shown in Figs. 1(a) and (b).

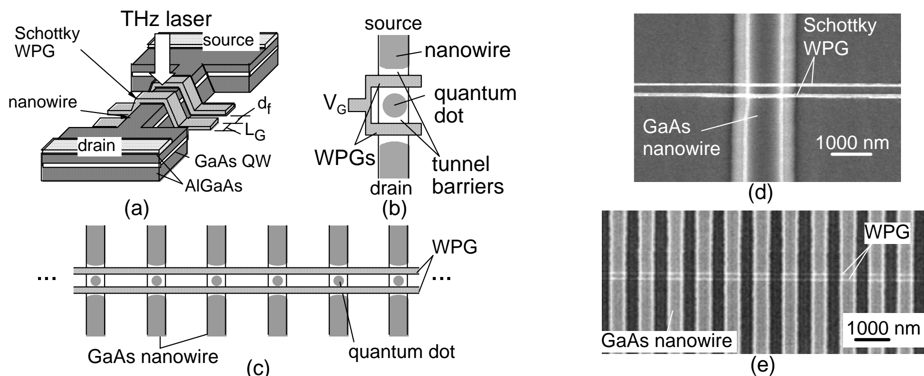


**Fig. 1** (a) Basic structures of WPG SET, (b) and (c) designs of single dot SET and parallel SET integration. (d) and (e) are SEM images of fabricated single dot SET and SET-integrated device, respectively.

Two nanometer-sized Schottky gates, wrapped around a GaAs nanowire with a narrow spacing, form double tunnelling barriers and a quantum dot in between. The barrier height and width, dot size and dot potential are controlled by the gate bias. In the dark, this structure operates as a single electron transistor (SET)[1]. The WPG with simple lateral structure is suitable for planar integration of quantum devices, as

*Corresponding author: kasai@rciqe.hokudai.ac.jp, Phone: +81-11706-7176, Fax: +81-11-716-6004



000000 physica (a) 193/3 WordXP Art.: W0000/Autor C:\Documents and Settings\Administrator\デスクトップ\葛西先生\ToDoWileyVCH\その他 3\QD02_G29+Fig.doc
&R31; insgesamt 4 Seiten Diskette 28.04.2006 Bearb.:

has been demonstrated recently by a novel hexagonal BDD quantum circuits [2]. In this study, THz response of single dot devices shown in Fig. 1(b) and an integrated device having 50 SETs in parallel shown in Fig. 1(c) were investigated.

**2 Experimental** GaAs nanowires, having wire widths of a few hundred nm, were fabricated on AlGaAs/GaAs heterostructure wafers by EB lithography and wet chemical etching. Cr/Au WPGs with a typical length of 85 nm were formed by EB lithography, metal deposition and lift-off process. SEM micrographs of completed devices are shown in Figs. 1(d) and (e).

Figure 2 shows the experimental set up. THz response of the WPG devices was measured by irradiating a THz (far infrared) laser beam at normal incidence on the samples using a $CH_3OH$ laser ($\lambda$ = 118 µm, $\nu$ = 2.54 THz). The sample was placed in a liquid He cryostat, and the SET drain current, $I_D$, was measured as a function of the gate voltage, $V_G$.

**3 Result and Discussion** Figure 3 shows measured $I_D$-$V_G$ characteristics of a single dot device with and without THz irradiation. In this figure, the nanowire direction was parallel to the electric field polarization of the THz wave as schematically shown in the figure. In the dark, the sample showed a single clear conductance peak followed by a rapid increase of current. The difference of the drain current, $\Delta I_D$, with and without THz irradiation is also shown in Fig. 3 as a function of $V_G$. Here, $\Delta I_D$ was obtained after extracting the exponentially increasing thermal current components from $I_D$ curve by fitting. With THz beam irradiation, the height of the first peak of the current decreased, showing a negative peak in $\Delta I_D$. At the same time, another positive broad peak appeared at a higher gate voltage in the $\Delta I_D$-$V_G$ plot. The height of the new peak in the $\Delta I_D$ plot was about 0.7 nA. When the nanowire direction was perpendicular to the polarization of the THz wave, no clear change of the current was seen.

The observed modulation cannot be due to thermally heating. In order to understand the experimental result, a theoretical analysis based on the photon assisted tunneling (PAT) theory[3,4] was attempted. Examples of calculated shape of the surrounding tunneling barrier profile and quantum dot are shown in Figs. 4 (a) and (b), respectively. In the dark, basic transport through such a structure can be

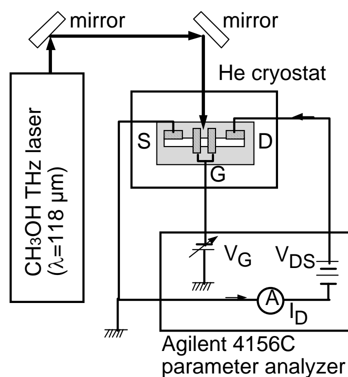


**Fig. 2** Measurement set up.

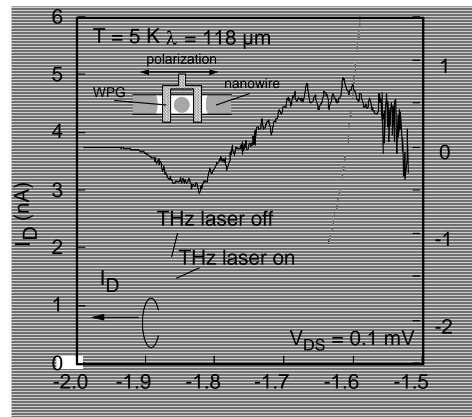


**Fig. 3** $I_D$-$V_G$ characteristics and $\Delta I_D$-$V_G$ curves.

explained by single electron resonant tunneling,
as we showed previously [1]. The observed rapid exponential increase of current after the single peak is due to thermal transport of electrons over the barriers. Then, the photon assisted tunneling probability, $T_{PAT}$(E), through this system, can be calculated by the following formula based on an analysis by Tien-Gordon Hamiltonian [3] on the THz irradiation,

$$T_{PAT}(E) = \sum_{n=-\infty}^{\infty} \frac{\Gamma_L \Gamma_R \left| J_n \left( qV_{ac}/h\nu \right) \right|^2}{\left( E - E_0 + nh\nu \right)^2 + \left( \Gamma/2 \right)^2} \quad (1)$$

where, $\Gamma_L$ and $\Gamma_R$ are the line width of the left and right tunneling barriers, $\Gamma = \Gamma_L + \Gamma_R$, $E_0$ is the quantized state in the dot, $J_n$ is Bessel function, $V_{ac}$ is amplitude of ac voltage induced by THz irradiation and $h\nu$ is THz photon energy. In this calculation, it was assumed, as a first approximation, that the tunnel barrier profile did not change as the Fermi level was swept with the gate voltage. The energy scale was translated to $V_G$ by $\Delta V_G = \Delta E/\alpha$ with $\alpha = 0.05$. The dependence of $\Gamma$ on the quantized energy level was considered and estimated from the calculation of tunneling probability using transfer matrix method. The current was calculated using the $T_{PAT}(E)$ in the conductance formula[1,5]where the currents of n = 0, ±1 for the first conductance peak was considered.

An example of the calculated current is shown in Fig. 5(a) for the cases with and without photo assisted tunneling. By THz irradiation, the main peak height decreased and an additional peak appeared at a higher gate voltage. A peak corresponding to n = -1 did not appear, since the energy becomes lower than the bottom of the dot potential for a large THz photon energy of $h\nu$ = 10.1 meV. Theoretical and experimental results are compared in Fig. 5(b) in terms of $\Delta I_D$-$V_G$ curves. Excellent agreements were obtained with the theoretical curve of $V_{ac}$ = 6 mV which seems to be reasonable from the intensity of laser beam. Thus, the experimental characteristics are due to PAT currents. The calculated temperature dependence of $\Delta I_D$-$V_G$ is also shown in Fig. 5(c). The PAT-induced second peak survives up to 30-50 K, whereas the negative peak quickly disappears and becomes positive, resulting in a single broad peak. This is due to the fact that thermal electrons can tunnel through n = +1 PAT channel at elevated temperatures even if the Fermi level lies at n = 0 position.

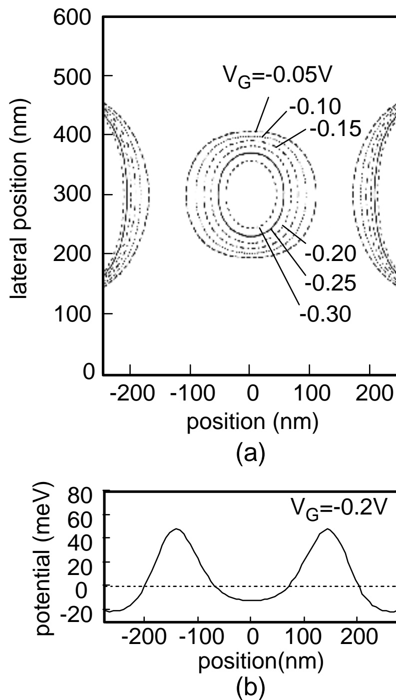


**Fig. 4** Potential simulation on WPG SET: (a) equipotential contour map and (b) potential profile.

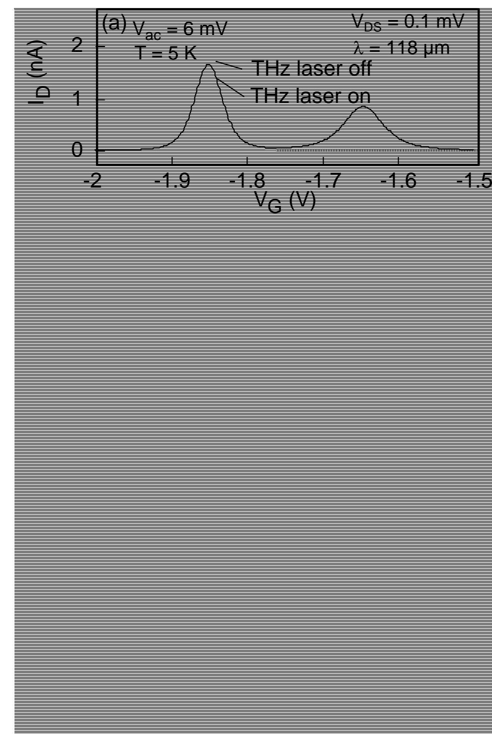


**Fig. 5** (a) Example of calculated current peaks by PAT. (b) and (c) are theoretical $\Delta I_D$-$V_G$ curves for various $V_{ac}$ and temperatures, respectively.

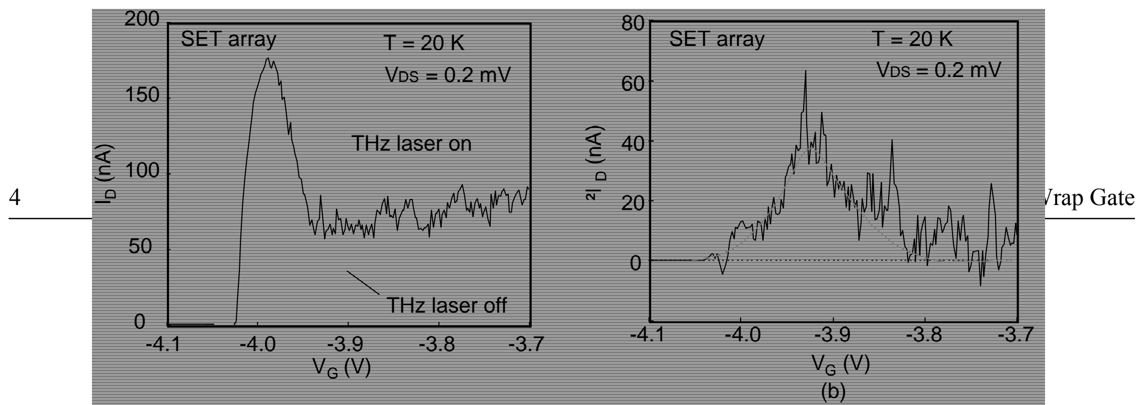


**Fig. 6** (a) $I_D$-$V_G$ and (b) $\Delta I_D$-$V_G$ characteristics of device integrating 50 WPGSETs in parallel.

The THz response of the integrated device having 50 SETs in parallel, measured at 20 K, is shown in Figs. 6(a) and (b). The PAT induced a new peak. Since the temperature was relatively high, only a single positive peak was appeared in the $\Delta I_D$-$V_G$, which is in qualitatively agreement with the result shown in Fig. 5(c). The peak has a large height of 38 nA which roughly corresponds to 0.7 nA x 50. This indicates that it is possible to increase the overall THz responsivity by forming large array of WPG SETs.

**4 Conclusions** THz responses of Schottky wrap gate (WPG)-controlled quantum dots were investigated. Normal incidence irradiation of THz beam on the single and integrated device surfaces using a $CH_3OH$ THz laser ($\nu$ = 2.54 THz) changed conductance behavior and produced an additional conductance peak at 5 - 20 K. Conductance change depended on the polarization of the beam, indicating the effect is induced by the THz electric field. The observed characteristics were explained by photon assisted tunnelling. As compared with the quantum well infrared photodetectors (QWIPs), the present device allows normal incidence of THz beams as well as high-density planar integration. The responsivity of the integrated device was high, being 0.3 A/W at 20K. Thus, it is promising for solid state THz detectors by enhancing the operation temperature with reducing device feature sizes.

## References


[1] S. Kasai and H. Hasegawa, Proc. of the 25th Int. Conf. on the Physics of Semiconductors, Part II (Springer, Berline, 2001) pp.1813-1814.

[2] S. Kasai and H. Hasegawa, IEEE Electron Device Lett. **23**, 446 (2002).

[3] P. K. Tien and J. P. Gordon, Phys. Rev. **129**, 647 (1963).

[4] L. P. Kouwenhoven, S. Jauhar, J. Orenstein, P. L. McEuen, Y. Nagamune, J. Motohisa and H. Sakaki, Phys. Rev. Lett. **73**, 3443 (1994).

[5] C. W. J. Beenakker, Phys. Rev. B **44**, 1646 (1991).


**Figure captions**

**Fig. 1** (a) Basic structures of WPG SET, (b) and (c) designs of single dot SET and parallel SET integration. (d) and (e) are SEM images of fabricated single dot SET and SET-integrated device, respectively.

**Fig. 2** Measurement set up.

**Fig. 3** $I_D$-$V_G$ characteristics and $\Delta I_D$-$V_G$ curves.

**Fig. 4** Potential simulation on WPG SET: (a) equipotential contour map and (b) potential profile.

**Fig. 5** (a) Example of calculated current peaks by PAT. (b) and (c) are theoretical $\Delta I_D$-$V_G$ curves for various $V_{ac}$ and temperatures, respectively.

**Fig. 6** (a) $I_D$-$V_G$ and (b) $\Delta I_D$-$V_G$ characteristics of device integrating 50 WPGSETs in parallel.